Laser and Particle Beams (2017), *35*, 492–504.

doi:10.1017/S0263034617000477

The effect of nature and pressure of ambient environment on laser-induced breakdown spectroscopy and ablation mechanisms of Si

K. ZEHRA,[1] S. BASHIR,[1] S.A. HASSAN,[2] Q.S. AHMED,[1,3] M. AKRAM,[1] AND A. HAYAT[1]

[1]Centre for Advanced Studies in Physics, Govt. College University, Lahore 54000, Pakistan
[2]Department of Energy Materials and Telecommunication, Institut national de la recherche scientifique (INRS), Québec, Canada
[3]Department of Electrical Engineering, Information Technology University (ITU), Lahore 54000, Pakistan

(Received 20 March 2017; Accepted 10 June 2017)

Abstract

The effect of nature and pressure of ambient environment on laser-induced breakdown spectroscopy (LIBS) and ablation mechanisms of silicon (Si) have been investigated. A *Q*-switched Nd-YAG laser with the wavelength of 1064 nm, pulse duration of 10 ns, and pulsed energy of 50 mJ was employed. Si targets were exposed under ambient environments of inert gases of argon, neon, and helium for different pressures ranging from 5 to 760 torr. The influence of nature and pressure of ambient gases on the emission intensity of Si plasma have been explored by using the LIBS spectrometer system. The plasma parameters such as electron temperature and number density were determined by applying Boltzmann plot and Stark broadening method, respectively. Our experimental results suggest that the nature and pressure of ambient environment play a significant role for generation, recombination, and expansion of plasma and consequently affect the excitation temperature as well as electron density of plasma. The surface morphological analysis of laser-irradiated Si was performed by using scanning electron microscope (SEM). Various kinds of structures, for example laser-induced periodic surface structures or ripples, cones, droplets, and craters have been generated and their density and size are found to be strongly dependent upon the ambient environment. A quantitative analysis of particulate size and crater depth measured from SEM images showed a strong correlation between plasma parameters and the growth of micro/nanostructures on the modified Si surface.

Keywords: Silicon; Laser-induced breakdown spectroscopy; Emission spectroscopy; Surface morphology; Periodic surface structures

1. INTRODUCTION

Laser-induced breakdown spectroscopy (LIBS) has been used for a variety of applications such as environmental monitoring, material analysis, thin-film deposition (Shabbir *et al*., 2017), micro-machining, nanostructuring, biological identification, and plasma characterization (Shaikh *et al*., 2006; Farid *et al*., 2012; Chen *et al*., 2013; Khan *et al*., 2013; Akram *et al*., 2014; Dawood *et al*., 2015). LIBS historically has been a qualitative technique, but over recent years it has been developed into a pseudo-quantitative materials microanalysis technique that is capable of determining the elemental composition of solids, liquids, and gases (Tognoni *et al*., 2002; Bogaerts *et al*., 2008; Cowpe *et al*., 2009; Shaikh *et al*., 2013).

In this technique, a pulsed laser source is employed to the target surface. The high intensity of the laser vaporizes the target forming a transient plasma or plume, which subsequently expands away from the sample surface (Shaikh *et al*., 2006). The plasma consists of neutrals, ions and electrons as well as excited species. The de-excitation of excited atoms generates the characteristic photons, which can be detected with optical emission spectroscopy (Chen *et al*., 2006). Multi-photon ionization and inverse Bremsstrahlung process (IB) lead to the excitation and ionization of investigated material resulting in high-temperature plasma formation (Shaikh *et al*., 2006; Cowpe *et al*., 2009; Farid *et al*., 2012; Khan *et al*., 2013; Akram *et al*., 2014). Laser-induced plasma parameters such as electron number density and excitation temperature are dependent upon various factors, for

Address correspondence and reprint requests to: S.A. Hassan, Department of Energy Material and Telecommunication, Institut national de la recherche scientifique (INRS), 1650, boulevard Lionel-Boulet Varennes (Québec) J3X 1S2, Canada. E-mail: hkazmi25@gmail.com

example the nature as well as pressure of background gases (Arshad *et al*., 2016), laser parameters (fluence, pulse width, wavelength, and spot size), physical and chemical properties of the target material. The plasma parameters can be determined from the emission spectrum of the plume (Cowpe *et al*., 2009; George *et al*., 2010).

The ambient environment plays a significant role for the evolution and expansion of laser-induced plasma. It has been observed that shape, size, and dynamics of the expanding plume are completely modified by introducing the ambient gas. The physical processes such as confinement effect, shielding effect (Tognoni *et al*., 2002; Giacomo *et al*., 2012), formation of shock waves (Giacomo *et al*., 2012), and the interaction of the plume with an ambient gas make plasma significantly important for various applications such as ion implantation using laser-induced plasma as ion source (Ahmed *et al*., 2016), pulse laser deposition of thin films (Bogaerts *et al*., 2008), and micro/nanostructuring of various kind of materials (George *et al*., 2010; Sobhani & Mahdieh, 2013). The growth of laser-induced surface structures is also strongly dependent upon the nature and pressure of ambient gas (Farid *et al*., 2012; Chen *et al*., 2013).The high value of excitation temperature and density of generated plasma lead to more energy deposition to the lattice of the target and enhances the growth of various micro/nanostructures on an irradiated surface.

Experiment with some similarities such as effect of ambient environment and influence of its pressure variation on the mass ablation rate, the plasma temperature, and the electron number density has been investigated by several groups (Kim *et al*. 1997; Cristoforetti *et al*., 2004) performed a quantitative analysis on Zn–Al alloy and observed that with the increase in ambient pressure of buffer gases the spectral emission intensities increases, and found more dominant in case of argon (Ar) ambience.

Mateo *et al*. (2012) described the effects of Air, Ar, and helium (He) ambience and pressure on LIBS intensity from several emission lines measured in samples such as brass, Cu, Al, and Si. In a very brief description, they concluded that the maximum emission intensity was observed for Ar ambience because of the lower ionization potential as compared with He. Shaik *et al*. (2006) determine the plasma parameters of Cd by the fundamental, second, and third-harmonic generations of Nd:YAG laser as well as the effect of pressure of ambience environment. Similarly from our previous group, a research conducted by Farid *et al*. (2012) highlighted the influence of ambient pressure and nature on Cd Plasma characteristics.

In more recent experiment, the importance of photoluminescence of Si nanocrystals with nanosecond laser ablation has been reported (Mahdieh & Momeni, 2014). Mahmood *et al*. (2010) explored the effects of laser parameters on nitrogen-assisted ablation of Si and revealed the formation of fibrous structures, which are responsible for the enhancement of optical absorption. While investigating the ablation mechanisms involved in surface modification and structural development on Si, only few contribution are reported describing the association between surface morphology and influencing parameters, for example effect of air and vacuum ambient on Si, laser-induced polarization, and double-pulse LIBS analysis of Si by the scientific community (Hayat *et al*., 2012; Penczak *et al*., 2012; Khalil, 2015). The spectroscopic analysis of Nd:YAG laser-induced Si plasmas in air at atmospheric pressure was performed by Liu *et al*. (1999).The generation and evolution of plasma during femtosecond laser ablation of Si are studied by steady-state and time-resolved spectroscopy in air, N_2, SF_6, and under vacuum (Chen *et al*., 2013). The surface density of sub-micron/nanoclusters and optical reflectivity of the irradiated Si were studied in terms of number of laser pulses and laser fluence (Sobhani & Mahdieh, 2013).

The aim of present work is to investigate the variation of nature and pressure of different ambient environments on emission spectroscopy of Si plasma. LIBS of Si (100) was carried out by exposing the target under ambient environment of inert gases of Ar, neon (Ne), and He for different pressures ranging from 5 to 760 torr by employing the LIBS technique. The plasma parameters such as electron temperature and electron number densities were determined by Boltzmann plot and Stark broadening method, respectively. The surface morphological analysis of laser-irradiated Si (100) was performed by scanning electron microscope (SEM). A correlation of excitation temperature and electron number density of plasma plume with the growth of surface structures of Si for various ambient environments have been evaluated and quantitatively justified by conducting a statistical analysis with the help of Gwyddion software.

2. EXPERIMENTAL DETAILS

Commercially polished single crystal Si (1 0 0) with dimensions of $10 \times 6 \times 1$ mm^3, were selected as target materials. Prior to laser treatment, these substrates were cleaned by sonication in acetone (15 min) and in isopropanol (15 min) before being dried under an Ar stream.

A linearly polarized Q-switched Nd:YAG (1064 nm, 10 ns, and 50 mJ) laser was employed for the ablation and plasma production. Before and after the experiment laser fluence was maintained at 2.4 J/cm^2. A schematic of experimental setup is shown in Figure 1. The plasma plume was evolved after focusing the incident laser beam by using a lens of focal length 50 cm. The incident beam propagation was perpendicular to the surface of the target. The Si targets were mounted on target holder under vacuum chamber (10^{-6} mbar). For fresh surface exposures, the target was rotated with the help of stepping motor to avoid non-uniform pitting and crater-formation. The radiations emitted from the Si plasma were collected by LIBS2500 (Broadband 200–980 nm, Resolution 0.1) plus spectrometer system (Ocean Optics, USA).The spectrometer system consisted of LIBS-Fiber bundle with seven Si CCD array detectors.

https://doi.org/10.1017/S0263034617000477 Published online by Cambridge University Press

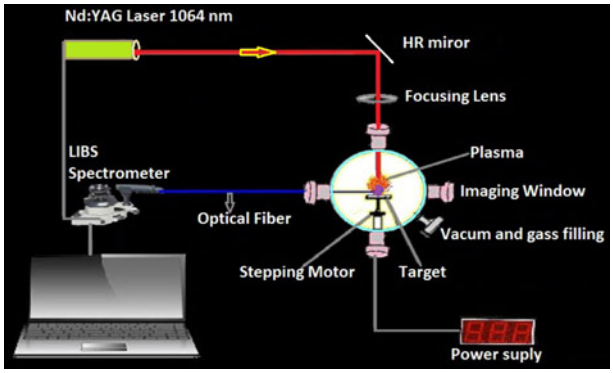

Fig. 1. The schematic representation of LIBS setup.

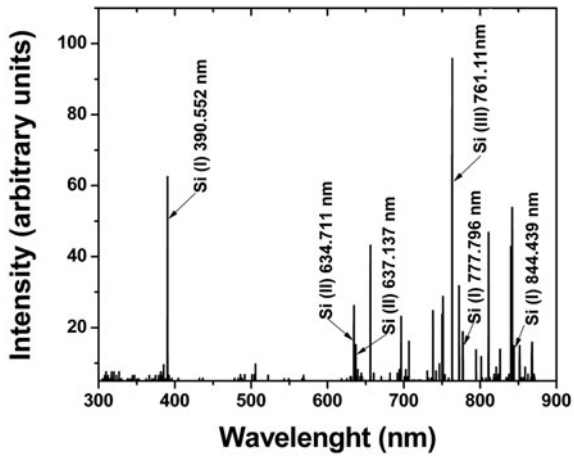

Fig. 2. The emission spectrum of laser-induced Si plasma under ambient environment of Ar at a pressure of 10 torr.

The data acquired to provide full spectral analysis by spectrometer was stored in a PC through OOILIBS software.

The delay time between the laser trigger and data collection was 1.25 μs, which was kept constant for all measurements. In order to investigate the effect of three inert gases Ar, Ne, and He were filled in the chamber one by one at various pressures ranging from 5 to 760 torr where the pressure could be controlled with mbar precision.

Two sets of experiments were performed. In the first set of experiment, laser beam with single shot hit the target. Plasma plume was generated inside the vacuum chamber and emissions were collected by LIBS spectrometer by using an optical fiber. In the second set of experiment, the target was exposed by 200 pulses of laser. Surface morphology of the laser-treated Si (1 0 0) was investigated by using SEM (JEOL JSM-6480 LV). Surface modifications were explored at the center and boundary regions of targets by using statistical analysis tool Gwyddion.

3. RESULTS AND DISCUSSION

3.1. Emission intensity

Figure 2 shows the emission spectra of Si plasma with spectral notation of Si (I), Si (II), and Si (III) representing the ionization stages one, two, and three of neutral and singly ionized Si species. The effect of nature and pressures of different ambient environments of Ar, Ne, and He on emission intensity of Si plasma is shown in Figure 3. This figure exhibits the variation in the emission intensity of all gases of Si for the pulse energy of 50 mJ and pressure ranging from 5 to 760 torr. The data is obtained for spectral transition lines of Si (I) from that shown in Table 1, which is evidently found in the previous literature (Khalil, 2015). It is observed that the intensity of emission spectrum initially increases with increasing pressure and attains its maxima at a pressure of 50 torr, and then decreases with further increase in pressure up to 760 torr. This behavior is same for all gases. However, the overall value of emission intensity of Ar is higher than those in Ne and He. It is found that the emission intensity is strongly dependent upon the pressure of ambient gases. For lower pressure, the free plasma expansion takes place and hence due to lower rate of excitation and de-excitation smaller intensities are observed. As pressure increases from 5 to 50 torr, the free expansion of plasma is restricted due to confinement effect (Akram *et al.*, 2014). This restricted expansion causes enhancement of collisional excitation and consequently the emission intensity increases. Further increase in pressure causes shielding effect (Giacomo *et al.*, 2012), and therefore emission intensity decreases. It shows that nature and pressure of ambient gases play an important role in the emission spectra of Si plasma.

3.2. Electron temperature

Two plasma parameters, electron temperature and number density are evaluated by the emission spectra of Si.

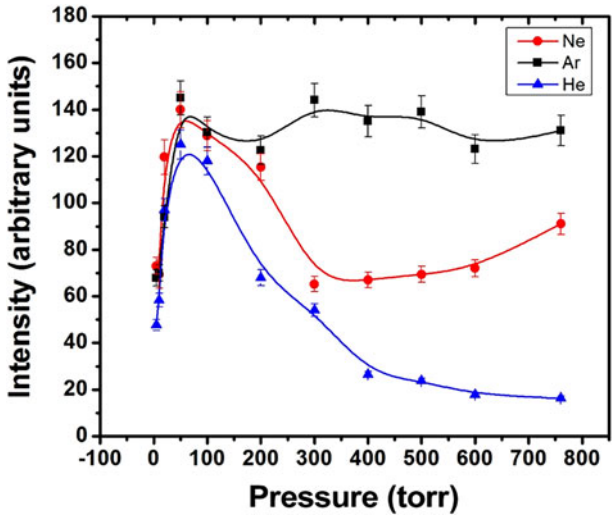

Fig. 3. The emission intensity of Si plasma under the ambient environments of Ar, Ne, and He.

https://doi.org/10.1017/S0263034617000477 Published online by Cambridge University Press

Table 1. *Spectroscopic parameters of Si lines used for the determination of excitation temperature and electron number density*

Element	Transitions	Wavelength [λ(nm)]	Transition probability (A) ($\times 10^8$ s^{-1})	Statistical weight (g_m)	Energy level E_m (cm)
Si(I)	$^1S_0$–$^1P^0$	390.552	0.118	3	40,992
Si(I)	$^3P^0$–$^1P^0$	777.796	0.000157	5	57,468
Si(I)	$^1D^0_2$–[1.5]$_2$	844.439	0.007	5	59,191

The emitted intensity of photons that is obtained due to excitation and de-excitation of electrons influence on electron temperature and number density of ionic and neutral species. For the determination of electron temperature, Boltzmann distribution has been employed, which is given by the following relation (Narayanan & Thareja, 2004; Shaikh *et al.*, 2006; Luo *et al.*, 2010):

$$\ln\left(\frac{\lambda_{mn} I_{mn}}{g_m A_{mn}}\right) = -\left(\frac{E_m}{KT_e}\right) + \ln\left(\frac{N(T)}{U(T)}\right), \quad (1)$$

where "λ_{mn}", "I_{mn}", and "A_{mn}" are the wavelength, intensity, and transition probability between m (upper state) and n (lower state), respectively. The "g_m" and "E_m" are statistical weight and energy of the upper state m. "$U(T)$" is the partition function, "$N(T)$" is the total number density, "k" is the Boltzmann constant, and "T_e" is the electron temperature. In order to determine the plasma temperature from Eq. (1), a Boltzmann plot of the logarithmic term ($\lambda_{mn} I_{mn}/g_m A_{mn}$) versus E_m for the observed spectral lines was applied that yields a straight line and its slope is equal to $-1/kT_e$ under the assumption of Boltzmann distribution.

Relevant spectroscopic parameters for transition lines of Si (I) has been taken from NIST database (Milan & Laserna, 2001). The overall evaluated value of electron temperature of Si plasma at various pressures (5–760 torr) for ambient environment of Ar, Ne, and He ranges from 2900 to 7000 K as shown in Figure 4. The observed highest value of electron temperature is for Ar, for Ne, and then for He. The values of electron temperature initially increase with increasing pressure, then attain their maxima, and then decrease by further increase in pressure. It is also observed that electron temperature attains its maxima at 500 torr for Ar, for Ne it is 200 torr, and for He it is 100 torr. It varies from 3087 to 6901 K for Ar, 3057 to 6204 K for Ne, and 2984 to 5419 K for He.

3.3. Number density

The electron density of Si plasma was determined by taking the consideration of the stark-broadening mechanism. The energetic-emitted species in plasma are directly influenced under the effect of electric field and consequently shift their energy levels. The Doppler line broadening is negligible as compared with the stark broadening. The electron density of the plasma related to stark broadening of the emission lines at full-width at half-maximum (FWHM) is given by the following relation (Shaikh *et al.*, 2006; Nakimana *et al.*, 2012).

$$\Delta\lambda_{1/2} = 2\omega\left(\frac{N_e}{10^{16}}\right) + 3.5A\left(\frac{N_e}{10^{16}}\right)^{1/4}\left[1 - 1.2{N_D}^{-1/3}\right] \times \omega\left(\frac{N_e}{10^{16}}\right), \quad (2)$$

where $\Delta\lambda_{1/2}$ is the FWHM broadening of the line, N_e is the plasma electron number density, w and A are the electron impact width parameter and the ion-broadening parameter, respectively, and N_D is the number density of particles in the Debye sphere given by equation (Shaikh *et al.*, 2007; Farid *et al.*, 2012).

$$N_D = 1.72 \times 10^9 \frac{T_e^{3/2}(\text{eV})}{N_e^{1/2}(\text{cm}^{-3})}. \quad (3)$$

The first term in Eq. (2) refers to the electron broadening and the second term is the contribution from ion broadening, which is very small in our case and can be neglected, and Eq. (2) reduces to (Milan & Laserna, 2001; Luo *et al.*, 2010).

$$\Delta\lambda_{1/2} = 2\omega\left(\frac{N_e}{10^{16}}\right). \quad (4)$$

The Lorentzian fit to the observed experimental data for the Si (I) transitions yields the FWHM. The thickness of the

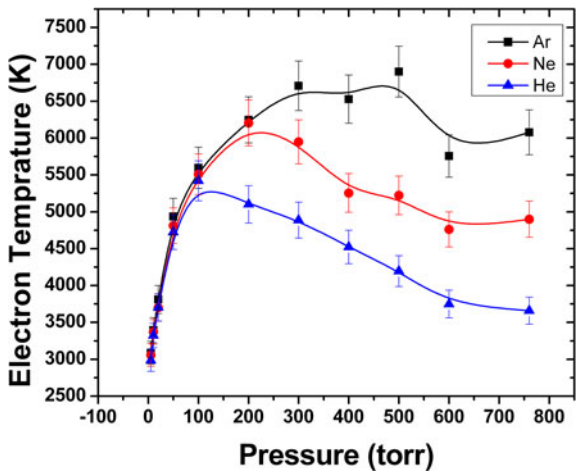

Fig. 4. The comparison of excitation temperature of Si plasma under ambient environments of Ar, Ne, and He for different pressures ranging from 5 to 760 torr.

https://doi.org/10.1017/S0263034617000477 Published online by Cambridge University Press

plasma is related to a complex interaction mechanism between the atoms/ions and the radiation, which is emitted and successively reabsorbed; the result on the spectra is the occurrence of self-absorption and a pronounced nonlinearity in the calibration function at increasing concentration (Bulajic *et al.*, 2002). The condition for the validity of the Local Thermodynamic Equilibrium is satisfied by using the following Mc-Whirter criteria (Shaikh *et al.*, 2006).

$$N_e \geq 1.6 \times 10^{12} T_e^{1/2} (\Delta E)^3, \quad (5)$$

where "ΔE (eV)" is the energy gap and "T_e" is the excitation temperature.

Figure 5 shows the resulting variation in the evaluated electron density of Si plasma for various pressures of Ar, Ne, and He. These values vary from 8.24×10^{17} to 9.70×10^{17} cm^{-3} for Ar, 8.01×10^{17} to 9.67×10^{17} cm^{-3} for Ne, and 7.79×10^{17} to 9.62×10^{17} cm^{-3} for He, under the pressures ranging from 5 to 760 torr. Initially the electron number density increases than decreases by further increasing in pressure upto 50 torr afterwards again increases and attains its maximum value at 500 torr for all ambient gases. Electron number density shows a slight diversion from the trend in the case of Ar at initial pressure.

3.3.1. Discussion

LIBS results show that nature and pressure of the ambient environments of Ar, Ne, and He significantly effects the plasma parameters, for example emission intensity, electron temperature, and electron number density. The observed highest value of emission intensity, electron temperature and electron density is for Ar, than Ne, and than for He. The values of emission intensity initially increases with increasing pressure and attains its maxima at 50 torr and then decreases by further increase in pressure for all ambient environments (Harilal *et al.*, 1998). Similarly the values of electron temperature, initially increases with increasing pressure and attains its maxima at 500 torr for Ar, 200 torr for Ne, 100 torr for He, and then decreases by further increase in pressure. While the electron number density for the ambient environments Ne and He, shows the decreasing trend upto 50 torr, and then increases by further increase in pressure. However, for the case of Ar a trivial nonlinearity in electron number density is observed, which appears in the form of hump (at low pressure). But remaining trend follows the same order as Ne and He do. This slight nonlinearity in electron number density with increasing pressure could be due to the lowest ionization potential of Ar as compared to Ne and He (Womer, 1931). The maximum value of electron number density for all gases Ar, Ne, and He are obtained at the pressure of 500 torr.

The initial increase in the emission intensity and excitation temperature is due to a rapid expansion of plasma and the electrons and ions collisions. For lower pressures, a large number of collisions between the expanding plasma and ambient atmosphere takes place (Akram *et al.*, 2014). When the pressure increases, the collisional frequencies of plasma species are enhanced by momentum transformation and cascade growth of electrons also increases (Farid *et al.*, 2012). The confinement effects also enhance the plasma parameters.

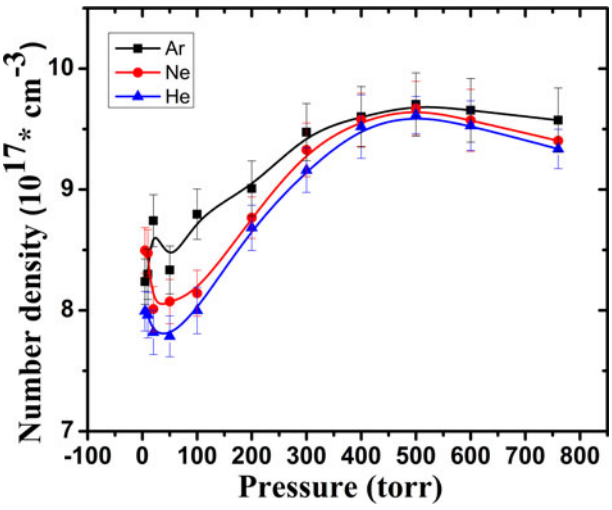

Fig. 5. The comparison of electron number density of Si plasma under ambient environments of Ar, Ne, and He for different pressures.

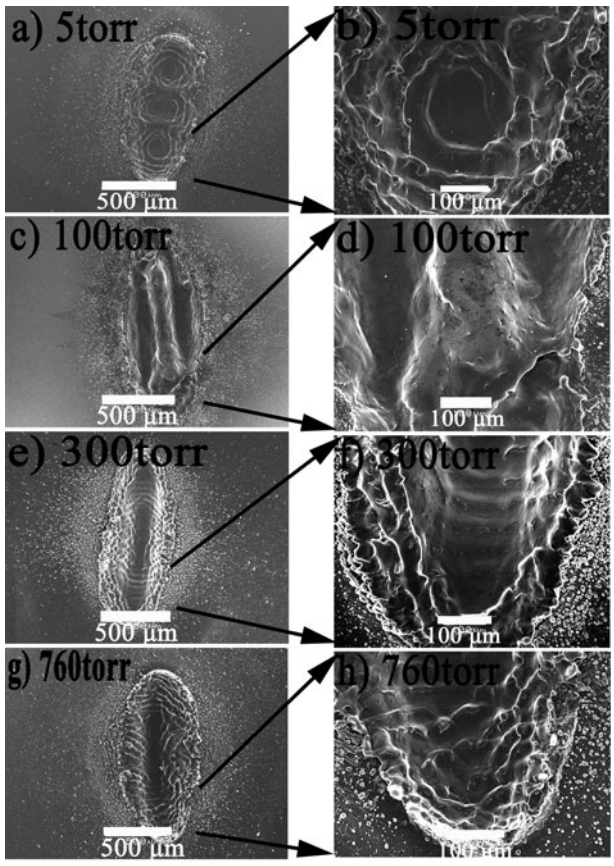

Fig. 6. SEM micrographs of laser-irradiated Si under the ambient environment of Ar at various pressures of 5 torr (a, b), 100 torr (c, d), 300 torr (e, f), and 760 torr (g, h).

https://doi.org/10.1017/S0263034617000477 Published online by Cambridge University Press

The breakdown of ambient gases serves as energy buffer and transfers its energy by thermal ionization, which increases the emission intensity, excitation temperature, and number density (Tognoni *et al*., 2002; Gondala & Khalil, 2012). As the pressure further increases upto 760 torr a strong confinement effect takes place, which in turns increases the frequency of elastic collisions of electron with the background gas. This results in a strong shielding effect that reduces the absorption of laser energy to the target surface and also reduces the ablated mass from the target. Therefore, the cascade condition is not favorable for high pressures, which supersedes the rate of growth of energy of free electrons via IB ionization, and results in low excitation temperature at high ambient pressures (Harilal *et al*., 1998; Tognoni *et al*., 2002).While in case of number density for low pressures initially the mean free path of ionized species is larger, therefore plasma expands more freely. As the pressure of the ambient gas increases, greater confinement of the plasma takes place, which enhances the elastic and inelastic collisions and thereby the recombination processes. This is supported by the fact that the initial increase in pressure decreases the electron density. Further increase in pressure enhances the number density, which is due to the increased number of particles per unit area as well as due to the fact that the energy gained by the recombination superseding the cooling due to increased intraplume collisions (Harilal *et al*., 1998).

It is observed that the nature of the gas also plays an effective role on plasma parameters as the line intensities in the Ar environment are much higher than those of Ne and He at the same pressure. This is due to the fact that the plasma expansion is slower in the heavy gas than the light gas due to its higher inertia (Shaikh *et al*., 2008, 2013; Gondala & Khalil, 2012), which keeps the plasma temperature high for a longer time and produces a strong plasma emissions. The other possibility is the plasma shielding, which is higher in the case of Ar because of its lower ionization potential than Ne and He (Iida, 1990).

The interaction between the expanding plasma and ambient gas causes the ionization of ambient gas, which contributes to the increase in electron density. The transfer of kinetic energy from the plasma plume to the background gas via Coulomb scattering and ion–neutral collisions is clearly

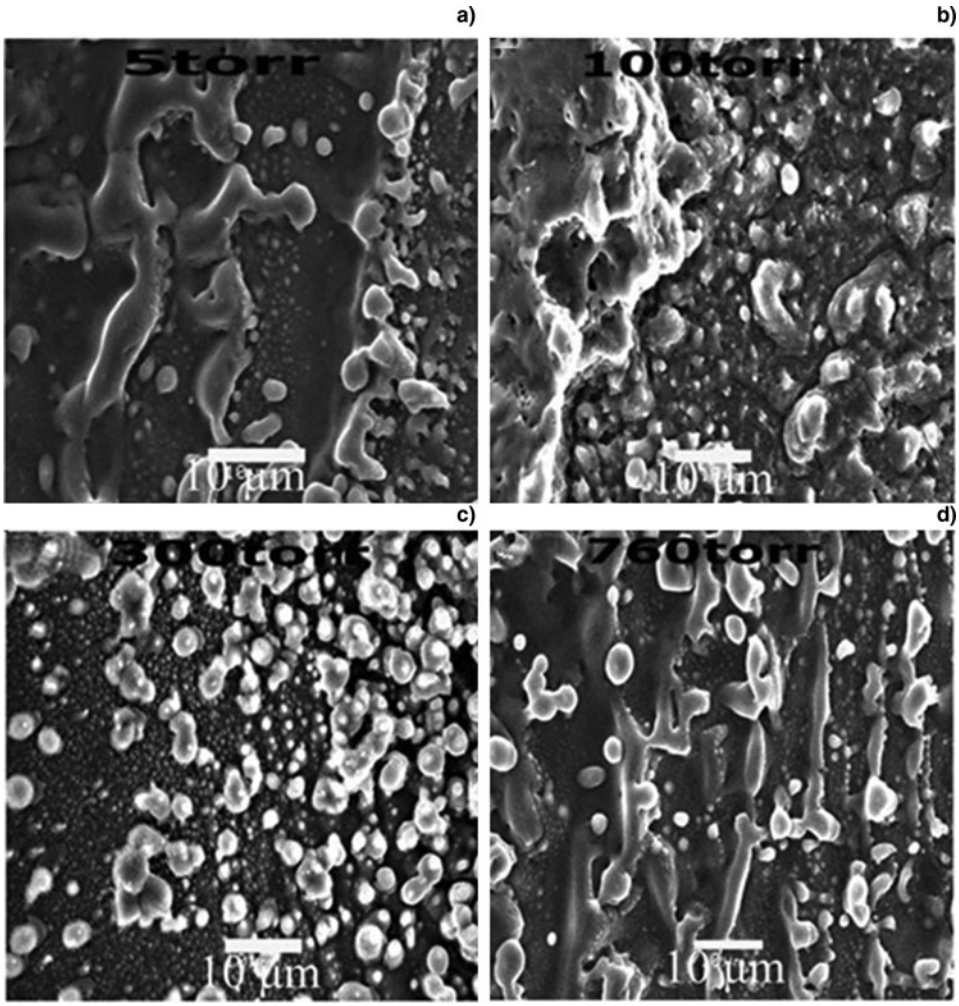

Fig. 7. SEM images revealing the surface morphology of grown nanoparticles at peripheral ablated area resulting from the laser irradiation of the Si under Ar environment at various pressures of: (a) 5 torr, (b) 100 torr, (c) 300 torr, and (d) 760 torr.

https://doi.org/10.1017/S0263034617000477 Published online by Cambridge University Press

observed at low-pressure regime of He (George *et al*., 2010). Since the ionization energy of He is greater than Ar and Ne, more increase in electron density is expected in Ar environment .It is clear from the results that Ar, Ne, and He exhibit the similar trend by giving the maxima at 500 torr (George *et al*., 2010). However, initially for all ambient environments, for the pressure upto 50 torr, a decreasing behavior is observed and this is due to the recombination losses of ions.

The nature of the background gas greatly influences the cascade growth of the electron by absorption of laser pulse. The necessary condition for the development of cascade like growth is given by (George *et al*., 2010; Farid *et al*, 2012).

$$\frac{d\varepsilon}{dt} = \frac{4\pi^2 e^2 I\, \upsilon_{\text{eff}}}{m_e c\omega^2} - \frac{2m_e \upsilon_{\text{eff}} E}{M}, \tag{6}$$

where ε is the free electron energy; *e* and *m* are the charge and the mass of an electron; *M* is the mass of the background gas; *E* is the first ionization energy of the gas; v_{eff} is the effective frequency of electron–neutral collision; *I* is the radiation intensity; and ω the frequency of the radiation.

The first term in the equation expresses the growth rate of the energy absorption by IB process, and the second term gives the maximum energy loss rate of plasma by cascade growth due to its elastic and inelastic collisions with the neutral gas particles (Iida, 1990).

The E/M is the decisive factor for calculating the energy loss in the cascade growth. The evaluated E/M for He is 6.14, for Ne is 1.07, and for Ar is 0.39. This means that the cascade condition is more favorable for Ar as compared with Ne and He atmospheres. Hence, the plasma formed in Ar atmosphere is more absorptive than that in Ne and He, which directly influences the values of electron temperature and number density (Farid *et al*., 2012).

The thermal characteristics of the ambient gas are also responsible for variation in plasma parameters of Ar, Ne, and He. The thermal conductivity (at 300 K in 10^{-3} W/m/K) of He (152) is large enough as compared with Ne (49) and Ar (18). Therefore, the plasma in He environment cools rapidly as compared with Ne and Ar, thus resulting in a low temperature of plasma in the He atmosphere.

The rate of change of electron temperature in the plasma depends upon the sum of three terms viz., elastic collision, electron heating due to collision excitation and de-excitation of metastable ions, and recombination of ions. The rate of loss of electron energy at short times is mainly influenced by the elastic collision term $Q_{\Delta t}$ and is given by (Harilal *et al*., 1998; George *et al*., 2010; Farid *et al*., 2012; Khan *et al*., 2013).

$$Q_{\Delta t} = \frac{2m_e}{M_B}\sigma_{ea} n_B \left[\frac{5kT_e}{\pi m_e}\right]^{1/2}, \tag{7}$$

where "σ_{ea}" is the elastic scattering cross section of the electrons, "M_B" and "n_B" are the mass and density of the background gas atoms, respectively. "*k*" is Boltzmann constant, "T_e" is electron temperature, and "m_e" is the mass of electron. Hence, the cooling process is inversely proportional to the mass, so that the lighter gases are efficient for rapid cooling. He being the lighter gas as compared with Ar and Ne gives rise to rapid cooling. Therefore, the minimum value of plasma temperature is achieved for a gas of minimum mass, that is He (Khan *et al*., 2013).

It is concluded from above results that plasma emission intensity, excitation temperature, and electron number density are strongly influenced by the nature and pressure of the ambient gases.

3.4. Surface morphology

SEM micrographs of Figure 6 show the surface morphology of central ablated regions of Si exposed to 200 pulses of Nd: YAG laser under the ambient environment of Ar, filled at various pressures of 5 torr (a and b), 100 torr (c and d), 300 torr (e and f), and 760 torr (g and h). In Figure 6, images labeled as (a, c, e, and g) illustrate the crater formation (an overall view), whereas images (b, d, f and h) represent the corresponding magnified view of the periphery of ablated crater for all ambient environments.

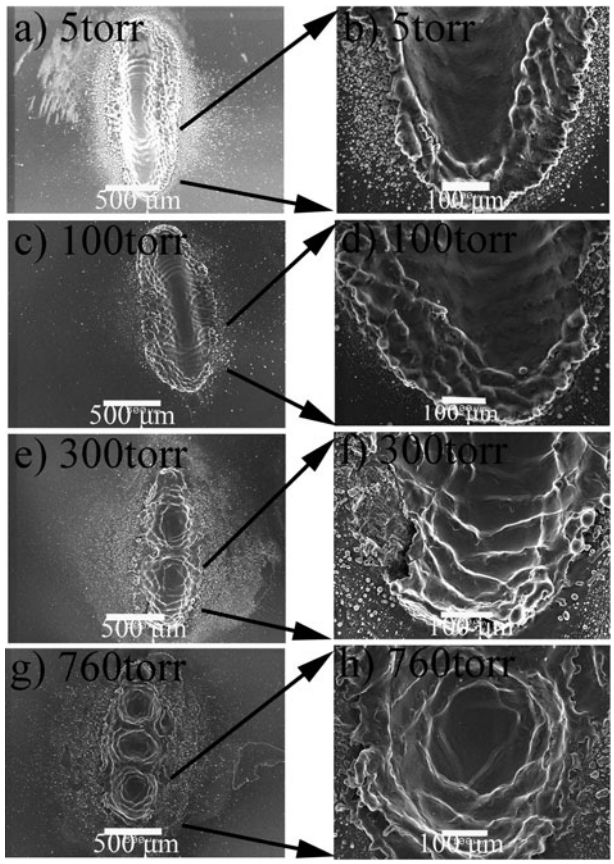

Fig. 8. SEM micrograph of laser-irradiated Si under the ambient environment of Ne at various pressures of 5 torr (a, b), 100 torr (c, d), 300 torr (e, f), and 760 torr (g, h).

https://doi.org/10.1017/S0263034617000477 Published online by Cambridge University Press

In case of Ar environment for the pressure of 5 torr, an elliptical crater is seen. This crater has been splitted up into three parts. One part of crater is magnified in Figure 6b in which laser-induced periodic surface structures (LIPSS) or ripples are grown. For the pressure of 100 torr in Figure 6c three distinct parts of crater are merged together and ripples are also vanished, which are seen in the magnified view of Figure 6d. By further increasing pressure upto 300 torr in Figure 6e various parts of the craters again indistinguishable, but ripples are again grow in both as well as in peripheral area of the crater and magnified in Figure 6f. The redeposition at the peripheries of crater also increases significantly for this pressure. When the pressure increases upto a maximum value of 760 torr, the width of crater increases and maximum number of distinct ripples are grown.

SEM images of Figure 7 labeled as (a, b, c, and d) show the magnified views of Figure 6b, 6d, 6f, and 6h at the boundaries at various filling of pressures (a) 5, (b) 100, (c) 300, and (d) 760 torr. For the pressure of 5 torr the liberation of micron-sized particulates and droplets, development of conical structures and globules are seen in Figure 7a. With the increase in pressure upto 100 torr in Figure 7b size and density of particulates, droplets, and cones increase. By further increase in pressure upto 300 torr in Figure 7c both the size and the density of particulates, spherical globules, and droplets increases significantly. However, large numbers of nano-sized particles are also seen. The transformation of droplets and particulates into channels is observed at the highest pressure of 760 torr is shown in Figure 7d.

SEM images of Figure 8 represent the modified surface morphology of Si after exposure to 200 laser pulses in the ambient environment of Ne. For the pressure of 5 torr inFigure 8a again an elliptical crater with LIPSS or ripples is seen, but no splitted part is observed as in the case of Ar environment. Ripples are seen in the magnified view of Figure 8b. For the pressure of 100 torr in Figure 8c the length of the crater decreases and width of crater slightly increases. The magnified view of ripples is shown in Figure 8d. By further increasing pressure upto 300 torr in Figure 8e the crater is splitted up into two parts. Lower part of the crater is

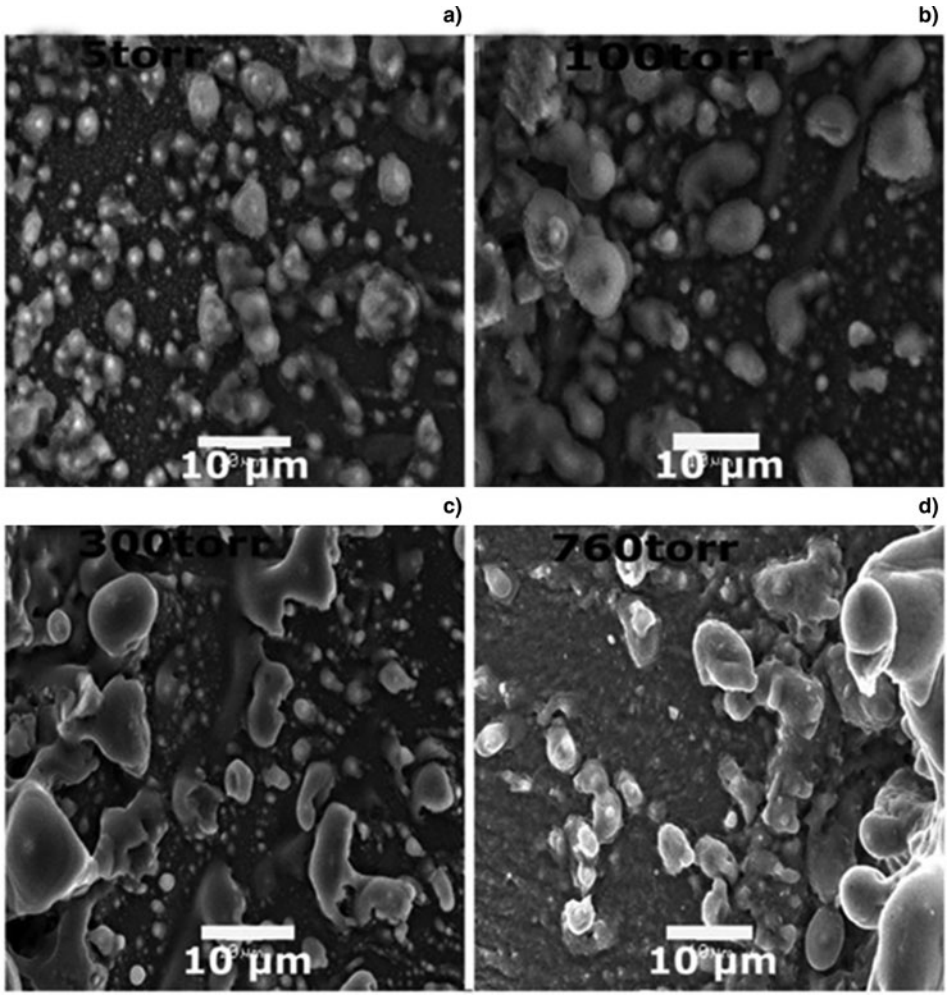

Fig. 9. SEM images revealing the surface morphology of grown nanoparticles at peripheral ablated area resulting from the laser irradiation of the Si under Ne environment at various pressures of: (a) 5 torr, (b) 100 torr, (c) 300 torr, and (d) 760 torr.

https://doi.org/10.1017/S0263034617000477 Published online by Cambridge University Press

magnified in Figure 8f in which micro ripples and cones are observed. When the pressure increases upto a maximum value of 760 torr, the crater is further splitted up into three parts as shown in Figure 8g. One part of the crater is magnified in Figure 8h in which ripples are also seen.

SEM images of Figure 9 represent the peripheries for different pressures of (a) 5, (b) 100, (c) 300, and (d) 760 torr. For the pressure of 5 torr in Figure 9a molten droplets and particulates are seen. The decrease in number density and increase in size of particulates and droplets are observed with the increasing pressure upto 100 torr in Figure 9b. At the pressure of 300 torr in Figure 9c size of particulates and droplets increases and some of these grow in the form of clusters with non-uniform size and density distribution. For maximum pressure 760 torr the the non-uniformly distributed droplets and particulates takes the elliptical and conical shape and their size distribution again reduces shown in Figure 9d.

SEM images of Figure 10 represent the modified surface morphology of Si after exposure to 200 laser pulses in the ambient environment of He. For the pressure of 5 torr in Figure 10a, an elliptical crater with diffused boundary is observed and magnified in Figure 10b. For the pressure of 100 torr in Figure 10c again an elliptical crater with larger size is seen. The ripples appearing at the boundary of crater become distinct, which is clear in the magnified view of Figure 10d. By further increasing pressure upto 300 torr in Figure 10e, the size of the crater further increases and ripples become more distinct as clearly seen in Figure 10f. When the pressure increases upto a maximum value of 760 torr in Figure 10f the crater boundary becomes diffused and ripples are almost vanished magnified in Figure 10h (Peng *et al.*, 2012).

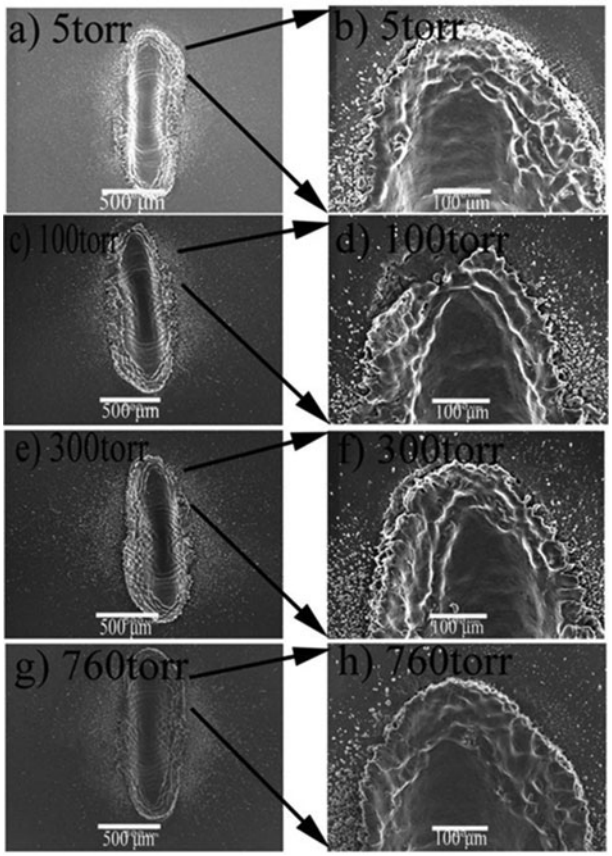

Fig. 10. SEM micrograph of laser-irradiated Si under the ambient environment of He at various pressures of 5 torr (a, b), 100 torr (c, d), 300 torr (e, f), and 760 torr (g, h).

SEM image of Figure 11 reveal the surface morphology of grown structures at various pressures of (a) 5, (b) 100, (c) 300, and (d) 760 torr. For the pressure of 5 torr in Figure 11a particulates, cones and droplets are observed. For the pressure of 100 torr in Figure 11b particulates and droplets are merged together and cones disappear. By further increase in pressure upto 300 in Figure 11c the size of molten droplets and particulates remains same. For a maximum pressure at 760 torr the droplets and particulates merge together and have been transformed into cone formation. Nanoparticles are also seen at the upper left periphery of the SEM image (Fig. 11d).

Upon irradiation with linearly polarized Nd:YAG (1064 nm) nanosecond laser pulses under normal incidence, usually two distinct types of LIPSS are observed, which are either parallel or perpendicular oriented to the beam polarization. In our case, LIPSS are observed in orientation perpendicular to incident laser beam polarization. These are generated by interference of the incident laser beam with a SEW (surface electromagnetic wave) generated on surface, which might include the excitation of SPPs (surface plasmon polaritons) (Bonse *et al.*, 2002; Bashir *et al.*, 2012; Behrenberg *et al.*, 2012). Surface defects, inhomogeneities, and capillary waves can also lead to the formation of ripples (Peng *et al.*, 2012). The formation of ripples is also explainable on the basis of the Kelvin–Helmholtz instability. When the pressure further increases the merging of the structures is caused by recondensation of the evaporated material on the surface and also depends upon the ambient pressure (Tognoni *et al.*, 2002; Farid *et al.*, 2012; Khan *et al.*, 2013). The appearance of LIPSS is more dominant in Ar than Ne and He due to the lower ionization potential of Ar gas and rapid cooling in He gas. Argon was found to be most efficiently heated by IB, generating buffer plasma, which optically shields the target surface, thus reducing the amount of ablated mass. The shielding effect also takes place in the presence of other gases (Iida, 1990). Growth of particulates, droplets, ripples, and periodic surface structures in the presence of inert gases environment is attributed to enhanced absorption of laser energy in the target surface (Wang *et al.*, 2007). For increasing pressure absorbed laser energy increases, the size of droplets and particulate increases, whereas the number of droplets and particulates decreases. The increase in surface absorption produces atomization and vaporization in the surface.

It is observed from the above Figures 6, 8 and 10 that the pressure of Ar, Ne, and He plays a significant role for the growth of structures on a Si surface. When a pulsed laser interacts with the Si surface, this results in the plasma formation. Due to increase in electron–ion collisions, the more energy transfer takes place and material temperature increases.

https://doi.org/10.1017/S0263034617000477 Published online by Cambridge University Press

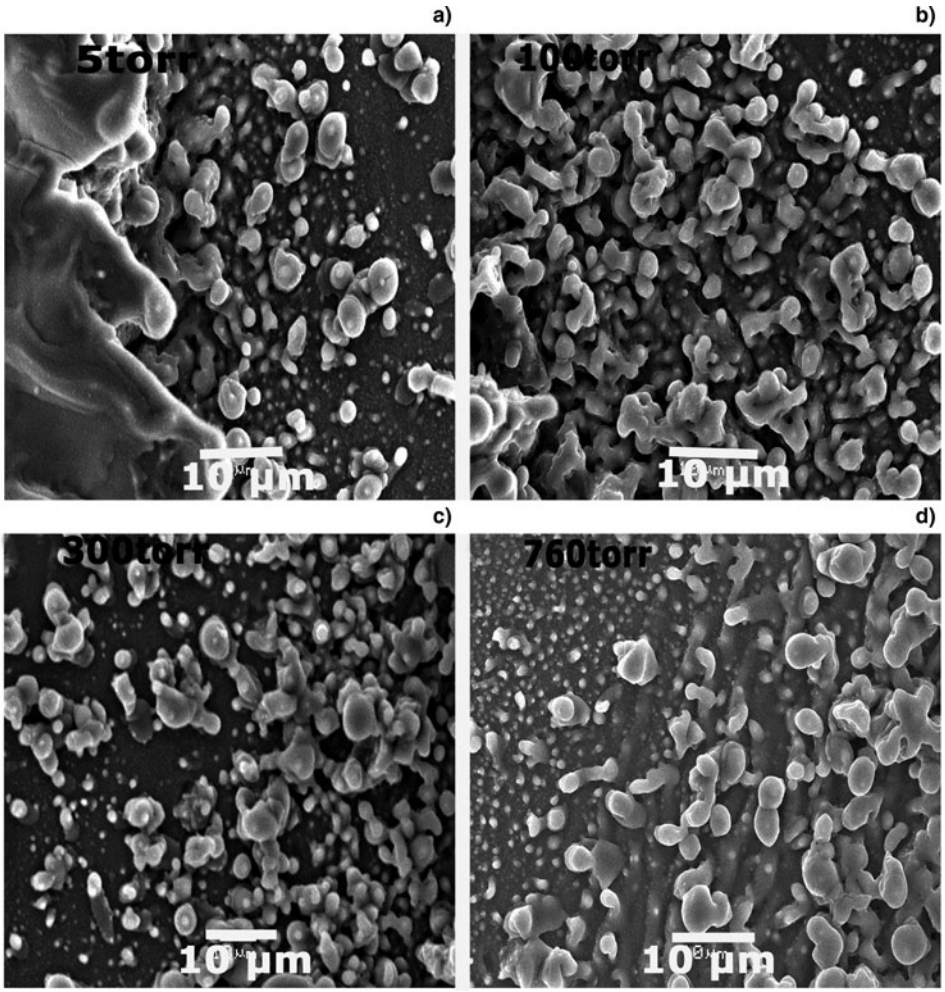

Fig. 11. SEM images revealing the surface morphology of grown nanoparticles at peripheral ablated area resulting from the laser irradiation of the Si under He environment at various pressures of (a) 5 torr, (b) 100 torr, (c) 300 torr, and (d) 760 torr.

Therefore, high-density and hot plasma is produced. When the pressure reaches upto 50 torr, the maximum value of excitation temperature causes the enhanced melting and ablation of Si as a consequence of the confinement of the vapor plasma, which prevents electrons or ion from rapidly escaping from the observation point and facilitate the atomization of droplets and particulates (Tognoni *et al*., 2002).Further increase in pressure the laser–material coupling efficiency is reduced by the plasma-shielding effect and the inclusion of ambient atmosphere that cools down the hot electrons by collisions, leading to a more efficient electron impact excitation and plasma recombination (Harilal *et al*., 1998), which in turn decreases electron number density and corresponding ripples and other structures are diminished. With further increase in pressure the number density increases so the corresponding ablation efficiency also increases.

3.5. Particulate size and crater depth analysis

Dependence of ambient gas pressure on emission signal of plasma induced with infrared laser pulses was studied and correlated with morphological features observed in SEM. Figure 12 represents a relationship between particulate size estimated from the SEM analysis and the effect of varying pressure of Ar, Ne, and He ambience. In Ar environment with the increase in pressure upto 100 torr, size and density of particulates are increased. By further increase in pressure upto 760 torr, linear trend is observed as both the size and the density of particulates increase significantly from 1.45 to 3.46 µm. Particle size increases from 3.52 to 5.50 µm under Ne ambience by increasing pressure from 5 to 100 torr, by further increasing the pressure (as previously discussed in Section 3.4) the size of particulates and droplets increases slightly which are clearly observable from Figure 9b, 9c, but at the maximum pressure of 760 torr the size of the particle size decreases to 4.8 µm. Under He environment at the initial pressure (5–100 torr) the particles are merging, which leads toward decrease in particles size from 2.16 to 1.92 µm. Further increasing the pressure from 300 to 760 torr, a slight increase in particles size increases, which interestingly agreed by observing Figure 11a–d.

https://doi.org/10.1017/S0263034617000477 Published online by Cambridge University Press

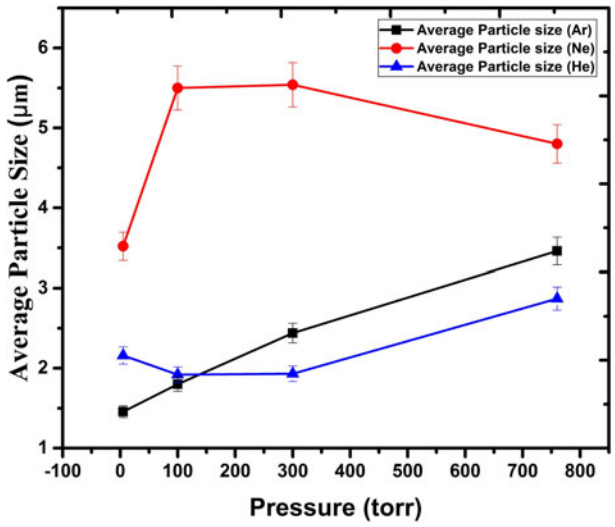

Fig. 12. The comparison of measured average particle size of laser-irradiated Si in ambient environments of Ar, Ne, and He for different pressures ranging from 5 to 760 torr.

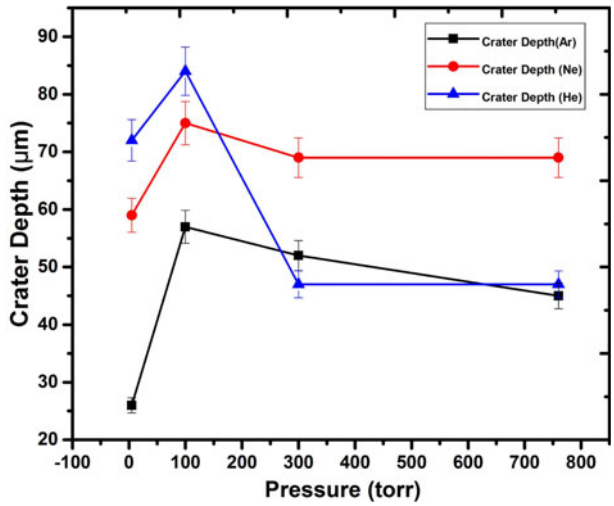

Fig. 13. The comparison of measured crater depth of laser-irradiated Si in ambient environments of Ar, Ne, and He for different pressures ranging from 5 to 760 torr.

Growth of particulates, droplets, ripples, and periodic surface structures in the presence of inert gases environment is attributed due to enhanced absorption of laser energy in the target surface (Wang, 2007). For increasing pressure absorbed laser energy increases, the size of droplets and particulate increases, while by further increasing in pressure the number of droplets and particulates decreases because of the saturation region arrived at this stage.

Figure 13 illustrates the information about increasing, decreasing, and saturation of craters depth of the ablated Si target by varying pressure in discussed ambience. It is worth mentioning that our statistical analysis obtained from SEM images is in good agreement with the theoretical estimation of intensity and electron temperature (Figs 3 and 4) as discussed in the previous section.

By increasing pressure from 5 to 100 torr, a prominent increase in crater depth in all ambient environments is observed. This increase in crater depth corresponds to enhance absorption of laser at lower pressure, resulting in large mass removal of Si target (also visible in SEM Figs 6b, 8b, and 10b). This pressure (100 torr) seems to constitute the best compromise between large amount of ablated material and a high electron temperature, resulting in the highest emission signal (as shown in Fig. 3).

However, a saturation, followed by a slight decrease, in the crater depth is observed by increasing the pressure to 760 torr. This can be attributed due to the energy losses of the plasma caused by the collisions with the buffer gas molecules, which increase with the buffer gas density and produce a faster decay of the temperature at the times considered for the measurements (Cristoforetti *et al.*, 2004). As it is being discussed that Ar has the lowest ionization potential than Ne and He, therefore plasma shielding effect will be the other possible reason of minimum crater depth (45 μm) compared with other.

4. CONCLUSIONS

The nature and pressure of the ambient environment have significantly influenced the emission intensity, excitation temperature, electron number density, and surface morphology. Initially excitation temperature increases with the increase in pressure, attains a maximum, and afterwards decreases with further increase in pressure. The initial increasing trend in emission intensity and electron temperature is due to the confinement effect. The decrease in electron temperature with further increase in pressure is attributed to shielding effect. Electron number density initially increases, then decreases, and finally increases with increasing pressure. This is again attributed to confinement, recombination, and enhancement of electron impact ionization. The maximum values of excitation temperature and electron number density are obtained from Ar and least from He. Morphological features such as particulate size and crater depth approximated by statistical analysis interestingly showed similar trends as concluded in our theoretical estimation of emission intensity and electron temperature. The surface modification of laser-irradiated target also depends upon the nature and pressure of an ambient gas and is correlated with the values of excitation temperature and electron density. These results show that the plasma characteristics and grown surface structures depend on the laser energy absorption, which is influenced by the confining and shielding effects of plasma and nature of ambient gases.

ACKNOWLEDGMENTS

We acknowledge Higher Education Commission of Pakistan for funding the project "Strengthening of Laser Facilities at GC University Lahore" Pakistan. We also acknowledge Asma Hayat, and Mahreen Akram for providing fruitful guidelines.

https://doi.org/10.1017/S0263034617000477 Published online by Cambridge University Press

REFERENCES

Ahmed, Q.S., Bashir, S., Jalil, S.A., Shabbir, M.K., Mahmood, K., Akram, M., Khalid, A., Yaseen, N. & Arshad, A. (2016). Surface, electrical and mechanical modifications of PMMA after implantation with laser produced iron plasma ions. *Nucl. Instrum. Methods Phys. Res B* **378**, 1–7.

Akram, M., Bashir, S., Hayat, A., Mahmood, K., Ahmad, R. & Khaleeq-U-Rahaman, M. (2014). Effect of laser irradiance on the surface morphology and laser induced plasma parameters of zinc. *Laser Part. Beams* **32**, 119–128.

Arshad, A., Bashir, S., Hayat, A., Akram, M., Khalid, A., Yaseen, N. & Ahmad, Q.S. (2016). Effect of magnetic field on laser-induced breakdown spectroscopy of graphite plasma. *Appl. Phys. B* **122**, 63.

Bashir, S., Rafique, M.S. & Husinsky, W. (2012). Femtosecond laser-induced subwavelength ripples on Al, Si, CaF_2 and CR-39. *Nucl. Instrum. Methods Phys. Res. B* **275**, 1–6.

Behrenberg, D., Franzka, S., Petermann, N., Wiggers, H. & Hartmann, N. (2012). Photothermal laser processing of thin silicon nanoparticle films: On the impact of oxide formation on film morphology. *Appl. Phys. A* **106**, 853–861.

Bogaerts, A., Chen, Z. & Autrique, D. (2008). Double pulse laser ablation and laser induced breakdown spectroscopy: A modeling investigation. *Spectrochim. Acta B* **63**, 746–754.

Bonse, J., Baudach, S., Krüger, J., Kautek, W. & Lenzner, M. (2002). Femtosecond laser ablation of silicon–modification thresholds and morphology. *Appl. Phys. A* **74**, 19–25.

Bulajic, D., Corsi, M., Cristoforetti, G., Legnaioli, S., Palleschi, V., Salvetti, A. & Tognoni, E. (2002). A procedure for correcting self-absorption in calibration free-laser induced breakdown spectroscopy. *Spectrochim. Acta B* **57**, 339–353.

Chen, Z., Bleiner, D. & Bogaerts, A. (2006). Effect of ambient pressure on laser ablation and plume expansion dynamics: A numerical simulation. *J. Appl. Phys*. **99**, 063304.

Chen, Z., Wu, Q., Yang, M., Tang, B., Yao, J., Rupp, R.A., Cao, Y. & Xu, J. (2013). Generation and evolution of plasma during femtosecond laser ablation of silicon in different ambient gases. *Laser Part. Beams* **13**, 1–7.

Cowpe, J.S., Pilkingtine, R.D., Astin, J.S. & Hill, A.E. (2009). The effect of ambirent pressure on laser-induced Si plasma temeperature, density and morphology. *J. Phys. D: Appl. Phys*. **42**, 165202.

Cristoforetti, G., Legnaioli, S., Palleschi, V., Salvetti, A. & Tognoni, E. (2004). Influence of ambient gas pressure on laser-induced breakdown spectroscopy technique in the parallel double-pulse configuration. *Spectrochim. Acta B* **59**,1907–1917.

Dawood, A., Bashir, S., Akram, M., Hayat, A., Ahmed, S., Iqbal, M.H. & Kazmi, A.H. (2015). Effect of nature and pressure of ambient environments on the surface morphology, plasma parameters, hardness, and corrosion resistance of laser-irradiated Mg-alloy. *Laser Part. Beams* **33**, 315–330.

Farid, N., Bashir, S. & Khaliq, M. (2012). Effect of ambient gas conditions on laser-induced copper plasma and surface morphology. *Phys. Scr.* **85**, 015702.

George, S., Kumar, A., Singh, R.K. & Nampoori, V.P.N. (2010). Effect of ambient gas on the expansion dynamics of plasma plumeformed by laser blow off of thin film. *Appl. Phys. A* **98**, 901–908.

Giacomo, D.A., Dell'Aglio, M., Gaudiuso, R., Amoruso, S. & Pascale, D.O. (2012). Effects of the background environment on formation, evolution and emission spectra of laser-induced plasmas. *Spectrochim. Acta B* **78**, 1–19.

Gondala, M.A. & Khalil, A.A.I. (2012). Effect of ambient conditions on laser induced breakdown spectra. *Laser Phys*. **22**, 1771–1779.

Harilal, S.S., Bindhu, C.V., Nampoori, V.P.N. & Vallabhan, C.P.G. (1998). Influence of ambient gas on the temperature and density of laser-produced carbon plasma. *Appl. Phys. Lett*. **72**, 167–169.

Hayat, A., Latif, A., Rafique, M.S., Khaleeq-ur-Rahman, M., Bhatti, K., Usman, A. & Rehman, A. (2012). Surface modifications of materials by repetitive laser pulses. *Radiat. Eff. Defects Solids* **167**, 403–409.

Iida, Y. (1990). Effects of atmosphere on laser vaporization and excitation processes of solid samples. *Spectrochim. Acta B* **45B**, 1353–1367.

Khalil, A.A.I. (2015). Chemical etching method assisted double-pulse LIBS for the analysis of silicon crystals. *Appl. Phys. A* **119**, 1087–1099.

Khan, S., Bashir, S., Hayat, A., Khaleeq-ur-Rahman, M. & Ul-Haq, F. (2013). Laser-induced breakdown spectroscopy of tantalum plasma. *Phys. Plasmas* **20**, 073104.

Kim, D., Yoo, K., Park, H., Oh, K. & Kim, D. (1997). Quantitative analysis of aluminum impurities in zinc alloy by laser-induced breakdown spectroscopy. *Appl. Spectrosc*. **51**, 22–29.

Liu, H.C., Mao, X.L., Yoo, J.H. & Russo, R.E. (1999). Early phase laser induced plasma diagnostics and mass removal during single-pulse laser ablation of silicon. *Spectrochim. Acta B* **54**, 1607–1624.

Luo, W.F., Zhao, X.X., Sun, Q.B., Gao, C.X., Tang, J., Wang, H.J & Zhao, W. (2010). Characteristics of the aluminum alloy plasma produced by a 1064 nm Nd:YAG laser with different irradiances. *Pramana – J. Phys*. **74**, 945–959.

Mahdieh, M. & Momeni, A. (2014). From single pulse to double pulse ns laser ablation of silicon in water: Photoluminescence enhancement of silicon nanocrystals. *Laser Phys*. **25**, 015901.

Mahmood, A.S., Venkatakrishnan, K., Tan, B. & Alubiady, M. (2010). Effect of laser parameters and assist gas on spectral response of silicon fibrous nanostructure. *J. Appl. Phys*. **108**, 094327.

Mateo, M., Piñon, V., Anglos, D. & Nicolas, G. (2012). Effect of ambient conditions on ultraviolet femtosecond pulse laser induced breakdown spectra. *Spectrochim. Acta B* **74**, 18–23.

Milan, M. & Laserna, J.J. (2001). Diagnostics of silicon plasmas produced by visible nanosecond laser ablation. *Spectrochim. Acta B* **56**, 275–288.

Nakimana, A., Tao, H., Camino, A., Gao, X., Hao, Z. & Lin, J. (2012). Effect of ambient pressure on femtosecond laserinduced breakdown spectroscopy of Al in Argon. *Int. Conf. on Optoelectronics and Microelectronics (ICOM*, Changchun University of Science and TechnologyChangchun, Jilin, China).

Narayanan, V. & Thareja, R.K. (2004). Emission spectroscopy of laser-ablated Si plasma related to nanoparticle formation. *Appl. Surf. Sci*. **222**, 382–393.

Penczak Jr., J.S., Liu, Y., Schaller, R.D., Rich, D.H. & Gordon, R.J. (2012). The mechanism for continuum polarization in laser induced breakdown spectroscopy of Si(111). *Spectrochim. Acta B* **74–75**, 3–10.

Peng, Y., Chen, H.Y., Zhu, C.G., Zhang, D.S., Zhou, Y.Y., Xiang, H. & Cai, B. (2012). The effect of laser wavelength on the

https://doi.org/10.1017/S0263034617000477 Published online by Cambridge University Press

formation of surface-microstructured silicon. *Mater. Lett*. **83**, 127–129.

Shabbir, M.K., Bashir, S., Ahmed, Q.S., Yaseen, N., Jalil, S.A., Akram, M., Mahmood, K. & Khalid, A. (2017). Effect of substrate temperature on the growth of copper oxide thin films deposited by pulsed laser deposition technique. *Surf. Rev. Lett*. **25**, 1850053–1850066.

Shaikh, M.N., Kalhoro, S.M., Hussaina, A. & Baig, A.M. (2013). Spectroscopic study of a lead plasma produced by the 1064 nm, 532 nm and 355 nm of a Nd:YAG laser. *Spectrochim. Acta B* **88**, 198–202.

Shaikh, N.M., Hafeez, S. & Baig, M.A. (2007). Spectroscopic studies of Ca plasma generated by the fundamental, second, and third harmonics of a Nd:YAG laser. *Spectrochim. Acta B* **62**, 1311.

Shaikh, N.M., Hafeez, S., Kalyar, M. A., Ali, R. & Baig, A.A. (2008). Spectroscopic characteristics of laser ablation brass plasma. *J. Appl. Phys*. **104**, 103108.

Shaikh, N.M., Rashid, B., Hafeez, S., Jamil, Y. & Baig, M.A. (2006). Measurement of electron density and temperature of a laser-induced zinc plasma. *J. Phys. D: Appl. Phys*. **39**, 1384–1391.

Shaikh, N.M., Rashid, B., Hafeez, S., Mahmood, S., Saleem, M. & Baig, M. (2006). Diagnostics of cadmium plasma produced by laser ablation. *J. Appl. Phys*. **100**, 073102.

Sobhani, M. & Mahdieh, M.H. (2013). Comparison of sub-micro/nano structure formation on polished silicon surface irradiated by nanosecond laser beam in ambient air and distilled water. *Laser Part. Beams* **13**, 1–9.

Tognoni, E., Palleschi, V., Corsi, M. & Cristoforetti, G. (2002). Quantitative micro-analysis by laser-induced breakdown spectroscopy: A review of the experimental approaches. *Spectrochim. Acta B* **57**, 1115–1130.

Wang, Y.L., Xu, W., Zhou, Y., Chu, L.Z. & Fu, G.S. (2007). Influence of pulse repetition rate on the average size of silicon nanoparticles deposited by laser ablation. *Laser Part. Beams* **25**, 9–13.

Womer, R. (1931). Ionization of helium, neon, and argon. *Phys. Rev*. **38**, 454.